

Geology, U-Pb geochronology, and geochemistry of the Miocene Pheno Mountain complex, Hoodoo Mountain area, British Columbia

A. Zagorevski^{1,a}, C. Dziawa², R.M. Friedman³ and M.G. Mihalynuk⁴

¹ Geological Survey of Canada, 601 Booth St., Ottawa, ON, K1A 0E8

² Department of Earth Sciences, Carleton University, Ottawa, ON, K1S 5B6

³ Pacific Centre for Isotopic and Geochemical Research, Department of Earth and Ocean Sciences, University of British Columbia, Vancouver, BC, V6T 1Z4

⁴ British Columbia Geological Survey, Ministry of Energy, Mines and Natural Gas, Victoria, BC, V8W 9N3

^a corresponding author: azagorev@nrcan.gc.ca

Recommended citation: Zagorevski, A., Dziawa, C., Friedman, R.M. and Mihalynuk, M.G., 2013. Geology, U-Pb geochronology, and geochemistry of the Miocene Pheno Mountain complex, Hoodoo Mountain area, British Columbia. In: Geological Fieldwork 2012, British Columbia Ministry of Energy, Mines and Natural Gas, British Columbia Geological Survey Paper 2013-1, pp. 115-125.

Abstract

The Pheno Mountain complex comprises rhyolite, trachyte and intrusive quartz feldspar porphyry that form extrusive and hypabyssal portions of a volcanic complex. A subvolcanic quartz feldspar porphyry with columnar jointing and brecciated margins underlies petrographically identical volcanic rocks. It yielded a 7.78 ± 0.01 Ma U-Pb zircon crystallization age, which is interpreted to constrain the age of the Pheno Mountain complex. Both the volcanic and hypabyssal rocks are characterized by high Nb/Y, Nb, Y, and Zr suggesting that they formed in a within-plate setting by fractional crystallization from an alkali basalt parent. These data support correlation of the Pheno Mountain complex with the Neogene to Quaternary Northern Cordilleran Volcanic Province. However, in contrast to the coeval Mount Edziza and Level Mountain volcanic centres, magmatism in the Pheno Mountain complex does not appear to be preceded by construction of a basaltic shield.

Keywords: Northern Cordilleran Volcanic Province, silica-saturated, felsic magmatism, alkaline rhyolite, peralkaline trachyte, upper Miocene, U-Pb geochronology, geochemistry

1. Introduction

The Neogene to Quaternary Northern Cordilleran Volcanic Province (NCVP) comprises predominantly alkaline volcanic rocks that extend from northwestern British Columbia to the Yukon-Alaska Border (Fig. 1). The NCVP erupted during dextral-oblique transtension of North America (Edwards and Russell, 2000). Over most of its geographical extent, the NCVP is dominated by short-lived, monogenetic mafic volcanic centres (see review in Edwards and Russell, 2000). A few centres, such as Level Mountain and Mount Edziza (Fig. 1), were long-lived and polygenetic. Well-dated strata of the Mount Edziza Complex, for example, indicate that the alkaline magmatism lasted from 7.5 Ma to Recent (Souther, 1992).

The NCVP extends through the Hoodoo Mountain Area (104/B14), where the conspicuous Late Quaternary (periods and epochs follow Gradstein et al. 2012) phonolitic Hoodoo Mountain Volcano erupted as recently as 9 Ka (Edwards et al., 2002). Neogene to Early Quaternary rocks have not been previously identified in this area. Mihalynuk et al. (2012) identified sections of volcanic and hypabyssal porphyritic rocks near Pheno Mountain (Pheno Mountain complex) ~ 15 km northwest

of Hoodoo Mountain (Fig. 2). Petrographic and geochemical data presented herein support that the volcanic and hypabyssal components of the Pheno Mountain complex are co-genetic. They are likely derived from fractional crystallization of a common alkali basalt parent. Our data demonstrate that Pheno Mountain complex is significantly older than the Hoodoo Mountain complex and is broadly coeval with the Late Miocene felsic volcanic rocks of the Mount Edziza, Level Mountain, and Heart Peaks complexes (Fig. 1).

2. Pheno Mountain complex

The Hoodoo Mountain region (104/B14) is characterized by mountainous terrain largely covered by the Andrei Glacier Icefield (Fig. 2). It is mainly underlain by Carboniferous to Jurassic volcanic, sedimentary and plutonic rocks that characterize the Stikine terrane (see Mihalynuk et al., 2011; Mihalynuk et al., 2012). These Mesozoic and older rocks are intruded by Eocene plutons of the Coast Plutonic Complex (Logan and Koyanagi, 1994) and are unconformably overlain and intruded by Neogene and younger rocks of the Northern Cordilleran Volcanic Province, such as the Late Quaternary phonolitic Hoodoo Mountain Volcano (Kerr, 1948; Edwards et al., 2002).

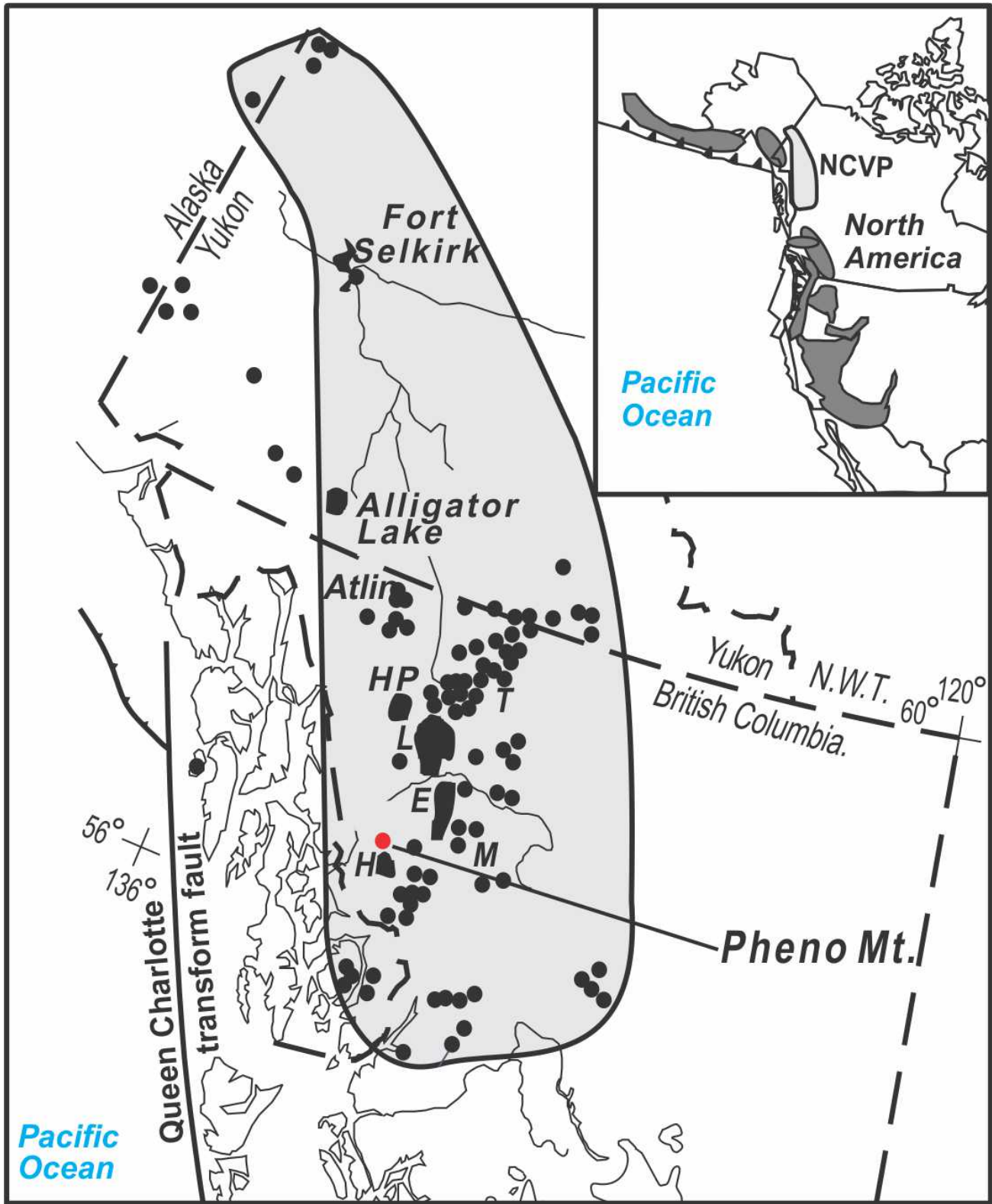


Fig. 1. Distribution of Neogene and Quaternary volcanic rocks of the Northern Cordilleran volcanic province (from Edwards and Russell, 2000) with location of the Pheno Mountain volcanic centre. E – Mount Edziza, H – Hoodoo Mountain, HP – Heart Peaks, L – Level Mountain, M – Maitland, T – Tuya. Inset: Location of the NCVP with respect to other Neogene and Quaternary volcanic rocks in western North America

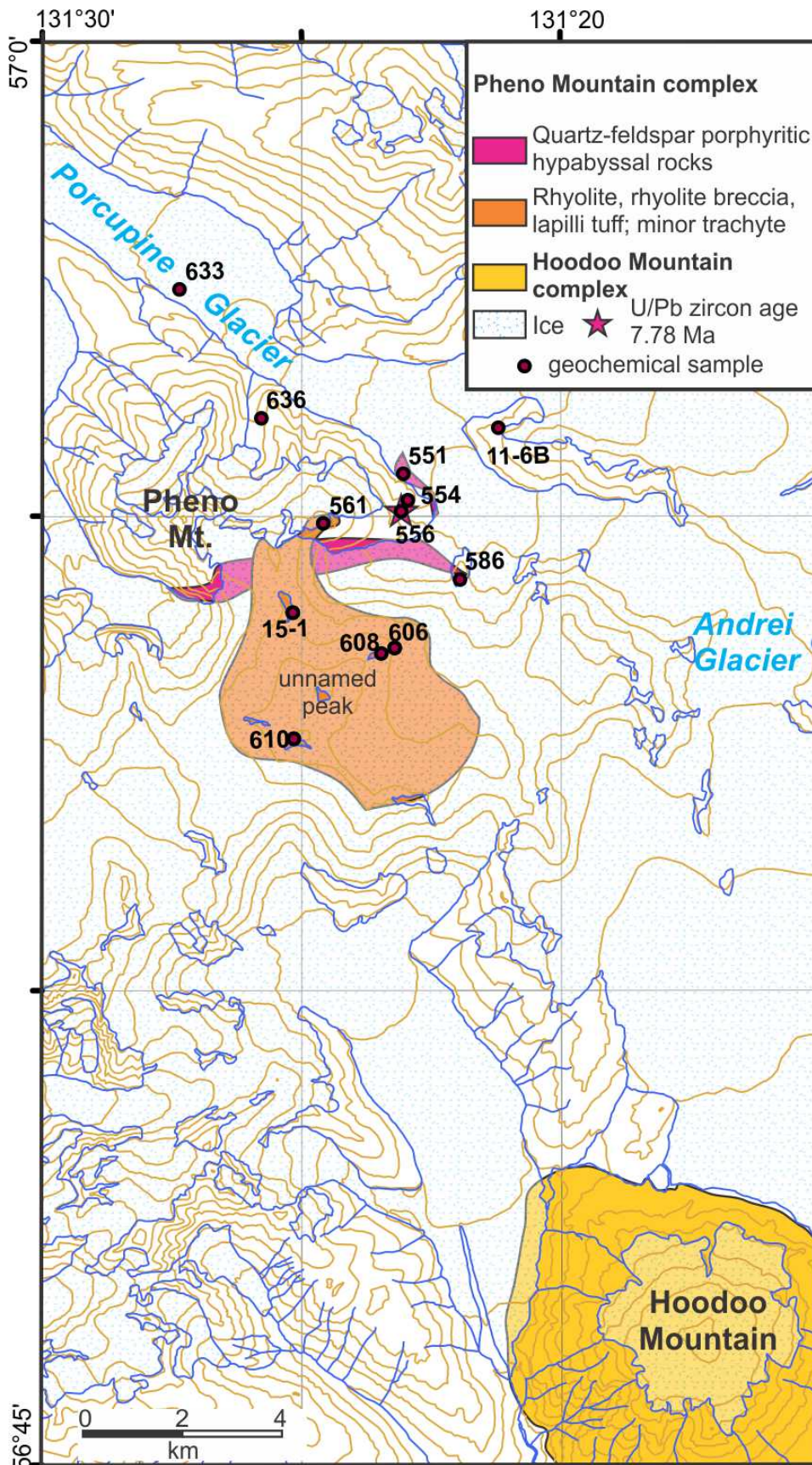


Fig. 2. Distribution of Neogene to Quaternary volcanic rocks in the Hoodoo Mountain area (modified from Mihalyuk et al., 2012).

The Pheno Mountain complex (Mihalynuk et al., 2012) is dominated by felsic to intermediate volcanic and hypabyssal rocks that are locally cut by mafic dikes. Exposures of the Pheno Mountain complex occur 15 km north-northwest of Hoodoo Mountain and Porcupine Glacier wraps north side of complex, about 1 km southeast of Pheno Mountain summit (Fig. 2). Large, rounded, rusty weathering boulders of the Pheno Mountain complex are common in the southern lateral moraine of Porcupine Glacier (Fig. 3a).

2.1. Volcanic rocks

Pheno Mountain complex volcanic rocks cap an unnamed peak 5 km SE of Pheno Mountain (Figs. 2, 3a-c). They predominantly comprise light blue-green to rusty, vesicular, quartz and feldspar porphyritic, rhyolitic lapilli tuff, tuff breccia, banded flows, and flow breccia (Fig. 3d). Dense pyroclasts commonly exhibit flow banding, coalesced spherulites, and perlite (Figs. 3e, f). Quartz phenocrysts (<3 mm, 5%) are euhedral to rounded and commonly embayed. Feldspar phenocrysts (<3 mm, <10%) locally contain zones of melt inclusions and are commonly altered. Some samples display granophyric intergrowth between quartz and alkali feldspar. Rare chloritized pseudomorphs suggest replacement of a mafic phenocryst phase, likely pyroxene (Fig. 3e). The vesicles are mostly open, though some are lined with opaque minerals or partly filled with chlorite.

2.2. Trachytic rocks

Feldspar porphyritic, macroscopically banded, trachytic rocks occur to the north of the main rhyolitic volcanic centre. The contact between the trachyte and rhyolite is obscured by extensive felsenmeer. Rhyolite and trachyte are interlayered (Fig. 3c); however, it is unclear whether trachytes are flows or sills. Trachyte does occur as 1 m wide, north-trending dikes (Fig. 2). Trachyte contains glomeroporphyritic or granophyric, locally sieve-textured feldspar (<10 mm). Clinopyroxene is locally present. One sample contains abundant fine grained, strongly coloured, pleochroic blue amphibole typical of peralkaline suites (Fig. 4d).

2.3. Felsic hypabyssal rocks

Felsic hypabyssal rocks are common near Pheno Mountain, immediately to the north of the volcanic rocks (Figs. 2, 3a, b). Other areas to the east, west and south are largely obscured by ice or were inaccessible during mapping. Petrographically similar north-trending dikes occur 13 km south of Pheno Mountain and felsic dikes are common in cliff exposures near Pheno Mountain, suggesting that hypabyssal magmatism was likely extensive. Felsic hypabyssal rocks are dominated by quartz and feldspar porphyritic, holocrystalline, granophyric felsic dikes (Figs. 4a, b). Euhedral to rounded and embayed quartz (<5 mm) comprises <20% of most dikes. Euhedral, lath-shaped, locally sieve-textured feldspar phenocrysts (generally <5 mm up to 2 cm) generally comprise 20-25% of these rocks. Rarely, feldspar forms glomeroporphyritic aggregates. Some

samples contain hematite, calcite and/or chlorite-filled vesicles. The dikes locally display brecciated margins and columnar jointing; both suggest shallow depth of emplacement (Fig. 3b inset).

2.4. Mafic dikes

Feldspar porphyritic, pilotaxitic, vesicular mafic dikes cut the felsic hypabyssal rocks. Feldspar phenocrysts are euhedral to rounded and sieve-textured (Fig. 4c). Calcite and chlorite-filled amygdalae are commonly up to 1 cm, although rare vesicles are >5 cm. Some feldspar crystals show distinct albite twinning. The fine-grained matrix is altered, mostly to chlorite and carbonate.

3. Geochronology

U-Pb geochronology was conducted at the Pacific Centre for Isotopic and Geochemical Research (PCIGR), University of British Columbia (Vancouver) using chemical abrasion thermal ionization mass spectrometry (CA-TIMS) procedure that is modified from Mundil et al. (2004), Mattinson (2005) and Scoates and Friedman (2008). Rock samples were processed using standard mineral separation procedures, followed by hand picking of zircons in alcohol. The clearest, crack and inclusion-free grains were selected, photographed, and annealed in quartz glass crucibles at 900°C for 60 hours. Annealed grains were transferred into 3.5 mL PFA screw-top beakers, ultrapure HF (up to 50% strength, 500 µL) and HNO₃ (up to 14 N, 50 µL) were added and caps are closed finger tight. The beakers were placed in 125 mL PTFE liners and about 2 mL HF and 0.2 mL HNO₃ of the same strength as acid within beakers containing samples were added to the liners. The liners were then slid into stainless steel Parr™ high pressure dissolution devices, which were sealed and heated to a maximum of 200°C for 8-16 hours (typically 175°C for 12 hours). Beakers were removed from liners and zircon was separated from leachate. Zircons were rinsed with >18 MΩ.cm water and subboiled acetone. Then 2 mL of subboiled 6N HCl was added and beakers were set on a hotplate at 80°-130°C for 30 minutes and again rinsed with water and acetone. Masses were estimated from the dimensions (volumes) of grains. Single grains were transferred into clean 300 µL PFA microcapsules (crucibles), and 50 µL 50% HF and 5 µL 14 N HNO₃ were added. Each was spiked with a ²³³⁻²³⁵U-²⁰⁵Pb tracer solution (EARTHTIME ET535), capped and again placed in a Parr liner (8-15 microcapsules per liner). HF and nitric acids in a 10:1 ratio, respectively, were added to the liner, which was then placed in a Parr high pressure device for 40 hours at 240°C. The resulting solutions were dried on a hotplate at 130°C, 50 µL 6N HCl was added to the microcapsules, and fluorides were dissolved in high pressure Parr devices for 12 hours at 210°C. HCl solutions were transferred into clean 7 mL PFA beakers and dried with 2 µL of 0.5 N H₃PO₄. Samples were loaded onto degassed, zone-refined Re filaments in 2 µL of silicic acid emitter (Gerstenberger and Haase, 1997).

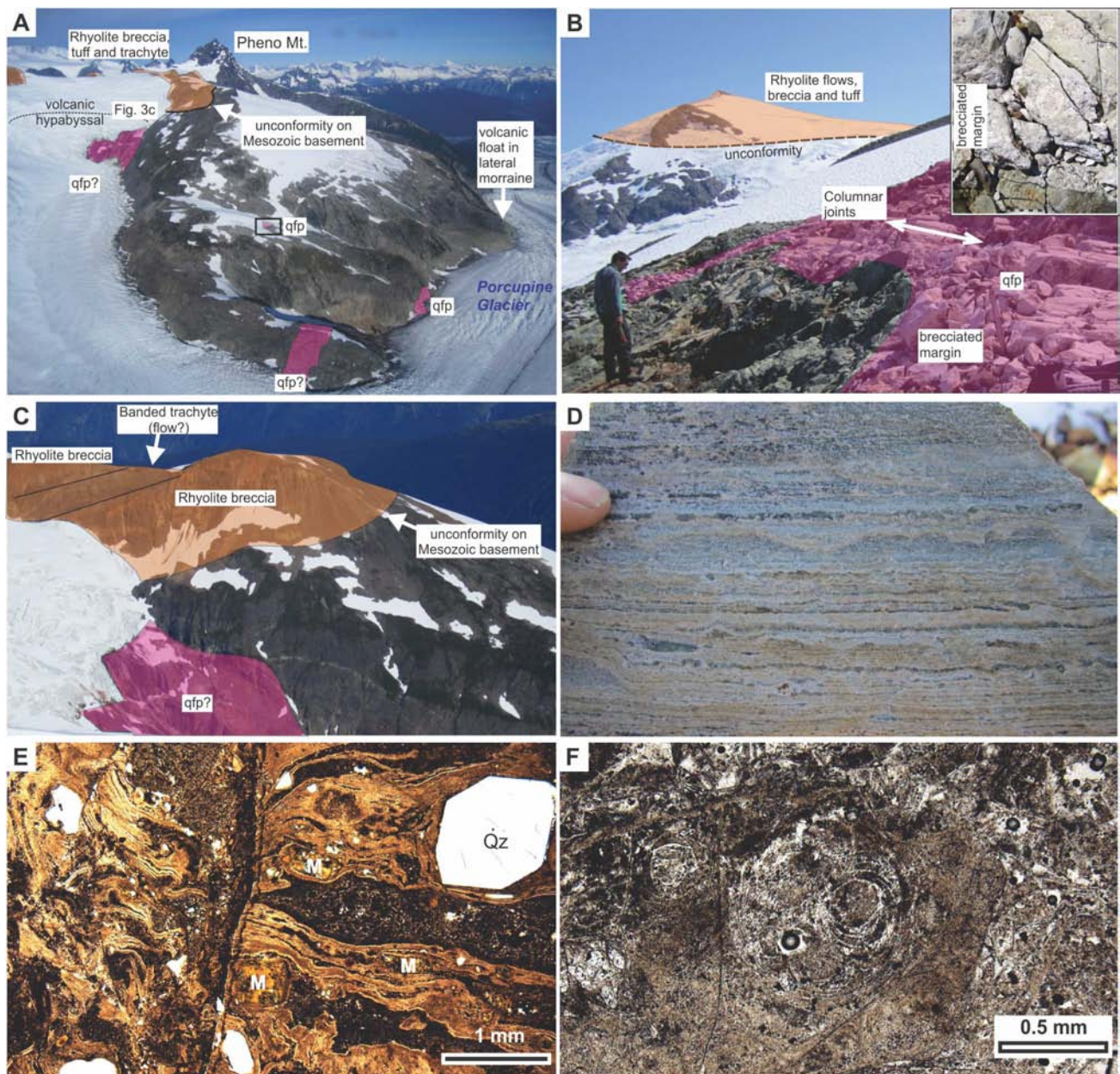


Fig. 3. Representative photographs of the Pheno Mountain complex. **a)** Relationships of Mesozoic basement with intrusive quartz and feldspar porphyric (qfp) and volcanic rocks, view to the WNW. Box marks the location of outcrop in **b)**. **b)** Dated locality (see Fig. 2) with intrusive columnar-jointed quartz and feldspar porphyry (foreground), view to the SW. Unnamed peak in the background is underlain by rhyolitic flows and breccia. Inset: margin of columnar-jointed dike displays fragmental texture, scale card graduations are 1 cm. **c)** Relationship between quartz and feldspar porphyry (qfp), rhyolite breccia and trachyte. Trachyte forms a banded, tabular body within rhyolitic rocks and may represent a flow or a sill, view to the N. Arrow identifying unconformity points to the same location as in Fig. 3a. **d)** Flow banded rhyolite with coalesced spherulites. **e)** Flow banded quartz (Qz)-phyric rhyolite with relict mafic phenocrysts (M). **f)** Perlitic fractures in rhyolite.

Isotopic ratios were measured on a modified single collector VG-54R or 354S (with Sector 54 electronics) thermal ionization mass spectrometer equipped with analogue Daly photomultipliers. Analytical blanks were 0.2 pg for U and 0.5 pg for Pb. U fractionation was determined directly on individual runs using the

EARTHTIME ET535 mixed $^{233-235}\text{U}$ - ^{205}Pb isotopic tracer and Pb isotopic ratios were corrected for fractionation of 0.23%/atomic mass unit, based on replicate analyses of NBS-982 reference material and the values recommended by Thirlwall (2000). Data reduction employed the Excel-based program of Schmitz and Schoene (2007). Standard concordia diagrams were constructed and weighted

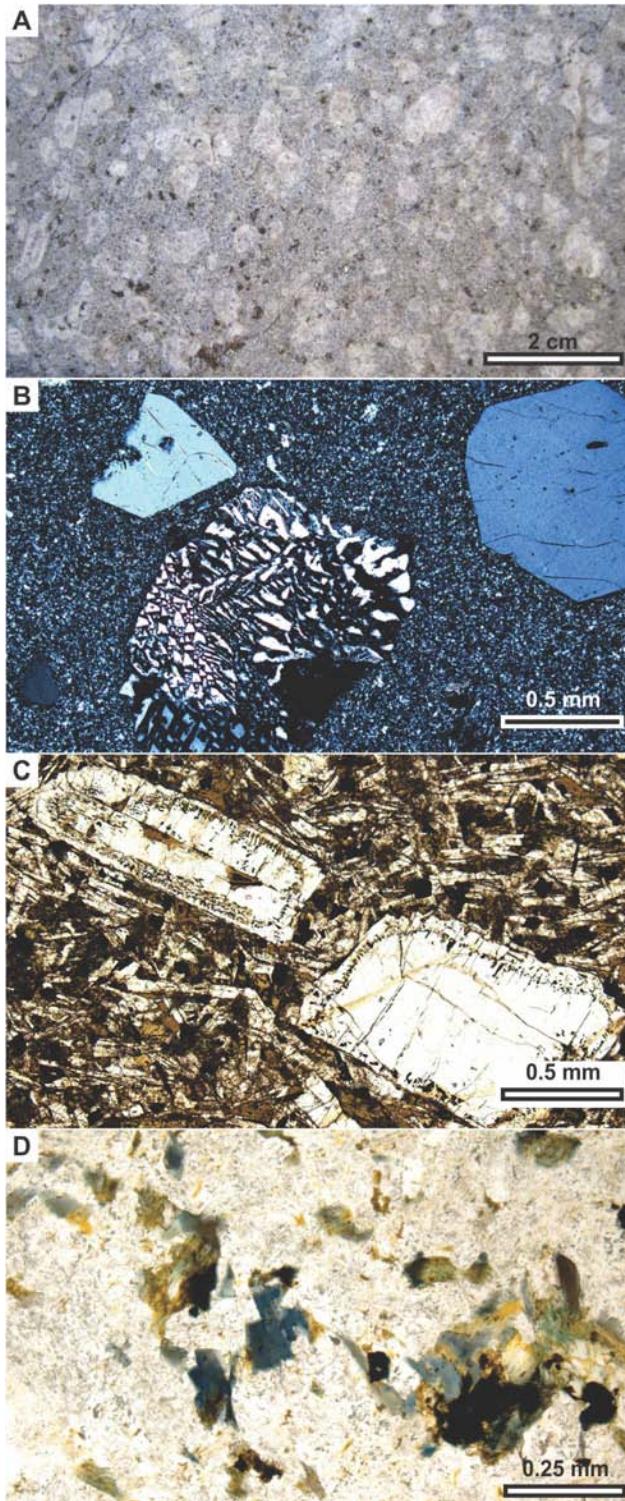


Fig. 4. Representative photographs of the Pheno Mountain complex. **a)** K-feldspar and quartz-phyric dike along the Porcupine Glacier. **b)** Photomicrograph of the dated quartz feldspar porphyry with granophyric crystals. **c)** Sieve-textured feldspar in mafic dike. **d)** Pleochroic, blue amphibole in trachyte dike.

$^{206}\text{Pb}/^{238}\text{U}$ age (2σ) calculated using Isoplot (Ludwig,

2003). Unless otherwise noted all errors are quoted as 2σ (95% confidence). Isotopic dates were calculated with the decay constants $\lambda_{238}=1.55125\text{E}-10$ and $\lambda_{235}=9.8485\text{E}-10$ (Jaffey et al., 1971).

3.1. Sample description and interpretation

A steep ridge south of Porcupine Glacier (Fig. 2) is dominated by bedded, moderately dipping, Mesozoic volcanogenic conglomerate and sandstone. The Mesozoic volcanogenic rocks are cut at a high angle to bedding by steep rhyolitic dikes. One dike exhibits well developed shallowly plunging columnar jointing that is perpendicular to the steep dike margin. Brecciation along the margin of this dike suggests very shallow level of emplacement (Fig. 3b). A sample from this dike (ZE11-556a; N56.91732, W131.38604) comprises light blue-green quartz and feldspar porphyritic, granophyric rhyolite. The sample yielded well-faceted, 150-200 μm stubby prismatic zircon grains with melt and apatite inclusions (Fig. 5 inset). Five single zircon grains were analyzed using CA-TIMS (Fig. 5). The three youngest grains yielded overlapping concordant data with a weighted $^{206}\text{Pb}/^{238}\text{U}$ age of 7.78 ± 0.01 Ma (MSWD = 0.52), which is interpreted to record the crystallization age of the columnar-jointed rhyolite dike. Two grains yielded $^{206}\text{Pb}/^{238}\text{U}$ ages of 7.92 ± 0.02 and 8.47 ± 0.01 Ma suggesting presence of an inherited, Cenozoic to Mesozoic component (Table 1).

4. Geochemistry

Sixteen samples of Pheno Mountain complex volcanic and hypabyssal rocks were screened for whole rock geochemical analysis using portable XRF (see Mihalynuk et al., 2012). The samples were trimmed to remove zones of weathering and alteration using a diamond saw. Major and trace elements were analyzed

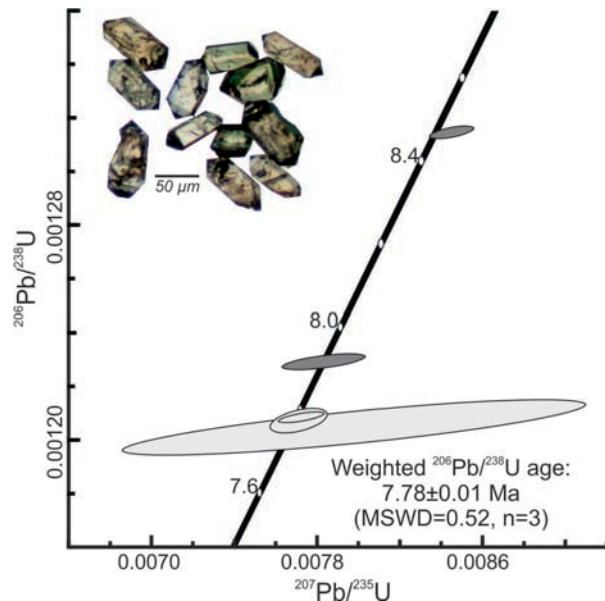


Fig. 5. U-Pb zircon concordia diagram of quartz feldspar porphyry. Inherited fractions are indicated by dark grey ellipses. Inset: Representative photomicrograph of analyzed zircon.

Table 1. U-Pb CA-TIMS analytical data for sample ZE11-556.

Sample	Compositional Parameters										Radiogenic Isotope Ratios						Isotopic Ages						
	Wt. mg	U ppm	Th ppm	Pb ppm	$x(10^{-13})$	$\frac{^{206}\text{Pb}^*}{^{206}\text{Pb}}$ mol %	$\frac{\text{Pb}^*}{\text{Pb}_c}$ (pg)	$\frac{^{206}\text{Pb}}{^{206}\text{Pb}}$ (f)	$\frac{^{206}\text{Pb}}{^{206}\text{Pb}}$ (g)	$\frac{^{206}\text{Pb}}{^{206}\text{Pb}}$ (g)	% err	$\frac{^{207}\text{Pb}}{^{235}\text{U}}$ (e)	% err	$\frac{^{206}\text{Pb}}{^{238}\text{U}}$ (g)	% err	$\frac{^{207}\text{Pb}}{^{206}\text{Pb}}$ (i)	corr. coef.	$\frac{^{207}\text{Pb}}{^{206}\text{Pb}}$ (i)	\pm	$\frac{^{206}\text{Pb}}{^{238}\text{U}}$ (j)	\pm	$\frac{^{206}\text{Pb}}{^{238}\text{U}}$ (h)	
A	0.0051	1177	0.318	1.5	0.2987	97.24%	10	0.70	673	0.104	0.046335	1.138	0.007717	1.229	0.001208	0.149	0.649	15.09	27.19	7.81	0.10	7.78	0.01
B	0.0063	1379	0.310	1.9	0.4710	97.71%	12	0.90	813	0.102	0.046643	0.979	0.008454	1.064	0.001315	0.159	0.588	31.01	23.34	8.55	0.09	8.47	0.01
C	0.0093	1121	0.324	2.7	0.5173	77.39%	1	12.46	82	0.110	0.048025	11.072	0.007973	11.645	0.001204	0.719	0.808	100.49	260.45	8.06	0.94	7.76	0.06
D	0.0112	1123	0.321	1.4	0.6251	98.34%	17	0.87	1121	0.105	0.046302	1.373	0.007704	1.497	0.001207	0.325	0.475	13.35	32.83	7.79	0.12	7.77	0.02
E	0.0491	162	0.342	0.2	0.4015	97.84%	13	0.72	857	0.111	0.046196	2.043	0.007827	2.166	0.001229	0.215	0.609	7.84	48.90	7.92	0.17	7.92	0.02

- (a) A, B etc. are labels for fractions composed of single zircon grains or fragments; all fractions annealed and chemically abraded after Mattinson (2005) and Scoates and Friedman (2008).
- (b) Nominal fraction weights estimated from photomicrographic grain dimensions, adjusted for partial dissolution during chemical abrasion.
- (c) Nominal U and total Pb concentrations subject to uncertainty in photomicrographic estimation of weight and partial dissolution during chemical abrasion.
- (d) Model Th/U ratio calculated from radiogenic $\frac{^{206}\text{Pb}}{^{206}\text{Pb}}$ / $\frac{^{206}\text{Pb}}{^{206}\text{Pb}}$ ratio and $\frac{^{207}\text{Pb}}{^{235}\text{U}}$ age.
- (e) Pb* and Pb_c represent radiogenic and common Pb, respectively; mol % $\frac{^{206}\text{Pb}^*}{^{206}\text{Pb}}$ with respect to radiogenic, blank and initial common Pb.
- (f) Measured ratio corrected for spike and fractionation only. Mass discrimination of 0.23%/amu based on analysis of NBS-982; all Daly analyses.
- (g) Corrected for fractionation, spike, and common Pb; up to 8 pg of common Pb was assumed to be procedural blank: $\frac{^{206}\text{Pb}}{^{206}\text{Pb}}$ / $\frac{^{206}\text{Pb}}{^{206}\text{Pb}}$ = 18.50 ± 1.0%; $\frac{^{207}\text{Pb}}{^{206}\text{Pb}}$ / $\frac{^{206}\text{Pb}}{^{206}\text{Pb}}$ = 15.50 ± 1.0%.
- (h) Errors are 2-sigma, propagated using the algorithms of Schmitz and Schoene (2007) and Crowley et al. (2007).
- (i) Calculations are based on the decay constants of Jaffey et al. (1971). $\frac{^{206}\text{Pb}}{^{206}\text{Pb}}$ / $\frac{^{206}\text{Pb}}{^{206}\text{Pb}}$ ages corrected for initial disequilibrium in $\frac{^{230}\text{Th}}{^{238}\text{U}}$ using Th/U [magma] = 3.

Isotopic dates are calculated the decay constants $\lambda_{238} = 1.55125\text{E}-10$ and $\lambda_{235} = 9.8485\text{E}-10$ (Jaffey et al. 1971).

using ICP-ES and ICP-MS following lithium metaborate/tetraborate fusion and nitric acid digestion (analytical package 4A4B) at ACME Laboratories (Vancouver, British Columbia). Whole-rock data are grouped on the basis of petrography (Table 2; Fig. 6).

4.1. Geochemistry results

Rhyolitic volcanic and hypabyssal rocks are characterized by high SiO₂ (72.3 to 80 wt.%), K₂O (2.2 to 7.5%), high Zr/Ti, high Nb/Y ratios and a peraluminous character. They plot in rhyolite and alkali rhyolite fields on discrimination plots (Figs. 6a, b). Most of the felsic rocks are characterized by high Zr (576 to 3110 ppm) and low Zr/Nb ratio (6.6 to 10.3). Heavy rare earth element (HREE) concentrations are 40 to 200 times chondritic values and LREE are moderately to strongly enriched (La/Yb - 3.2 to 13.1). Nb/Nb* ratios are variable (0.65 to 1.95). However, in many samples, Nb is enriched relative to La. Eu is strongly depleted (Eu/Eu* - 0.10 to 0.25) in both volcanic and hypabyssal samples, whereas Sr is highly depleted in volcanic samples (Sr 4.8 to 8.8 ppm). The dated sample (ZE11-556) exhibits a strong positive Ce anomaly (Ce/Ce* = 2.5), a strong negative Eu anomaly (Eu/Eu* = 0.04), and has a lower Zr/Hf ratio than other felsic samples (18 compared to 39).

Trachytic rocks (SiO₂ 59.8 to 61.8%) are characterized by lower Zr/Ti and similar Nb/Y ratios as the felsic rocks (Fig. 6b). They plot in the trachyte field on the TAS plot (Fig. 6a). They are characterized by high Zr (359 to 471 ppm) and low Zr/Nb ratio (7.5 to 8.5). They exhibit similar extended trace element profiles as the felsic rocks, but have generally lower absolute trace element abundances and a smaller Eu anomaly (Eu/Eu* - 0.63 to 0.78). The trachytic samples possess similar Zr/Hf ratios ($\mu = 40$) as the felsic rocks ($\mu = 39$). The sample that contains blue amphibole (ZE11-586) is acmite normative.

The mafic dike has high TiO₂ (2.5 wt.%) and Fe₂O_{3 total} (13.45 wt%), and plots near the boundary of the alkali basalt field (Fig. 6b). It exhibits similar extended trace element profile as the felsic and trachytic rocks, but has lower absolute trace element abundances and lacks Eu, Ti, and Sr depletion (Eu/Eu* = 1.03).

5. Summary and discussion

Regional mapping in the Hoodoo Mountain area identified a new felsic volcanic centre related to the Neogene to recent Northern Cordilleran Volcanic Province (Mihalynuk et al., 2012). The Pheno Mountain complex consists mainly of silica-saturated volcanic and hypabyssal rocks with minor metaluminous to peralkaline trachyte and alkali basalt. The petrography, geochemistry, and spatial co-occurrence of the felsic volcanic rocks and the stratigraphically underlying (Figs. 2, 3, 7) quartz and feldspar porphyritic hypabyssal rocks suggest that the rocks of the Pheno Mountain complex are co-genetic and represent parts of the same Miocene volcanic centre. Trachytic rocks are locally interlayered with the felsic volcanic rocks and may be either coeval or younger,

depending on whether the relationship is stratigraphic or intrusive. The age of the mafic and trachytic dikes is only constrained as younger than the hypabyssal porphyries.

Trace element geochemistry supports including the volcanic and hypabyssal rocks in the same magmatic suite. Both rocks are characterized by similar Nb/Ti ratios but different Zr/Ti ratios (Fig. 6b) suggesting that the compositional range resulted from fractionation of a parental magma similar to the mafic dike. This interpretation is supported by deeper Eu* anomalies with increasing Zr/Ti ratios (not shown), which suggest feldspar fractionation. The dated sample has similar characteristics, but contains a positive Ce anomaly, a more pronounced Eu anomaly, and overall lower LREE than other samples. These characteristics are easiest attributed to fractionation of LREE-rich phases, such as apatite, or volatile-mediated mobility of LREE complexes in a shallow magma chamber.

Trace element characteristics such as strongly enriched Nb, Zr, and Y (Figs. 6d, e) are all typical of within-plate magma suites (Fig. 6c) that form predominantly by fractionation of alkali basalt parental magma (e.g., Souther, 1992; Edwards et al., 2002; Macdonald, 2012). However, in contrast to typical within-plate highly fractionated peralkaline rhyolites, the Pheno Mountain complex rhyolite and hypabyssal quartz and feldspar porphyries display an alkalinity and alumina-saturation index typical of peraluminous rocks ($Al/(Na+K) > 1$ and $Al/(Ca+Na+K) \geq 1$).

The alkalinity index is very sensitive to mobility of alkali elements, whether in a shallow magma chamber, during cooling (e.g., Noble, 1970) and/or due to post-emplacement fluid-rock interaction. Many of our samples show evidence of fluid interaction (replacement of matrix and infilling of amygdals). Our samples also display non-systematic variation in concentrations of Na₂O and K₂O (Table 2), suggesting mobility of elements used in alkalinity and alumina-saturation indexes. Relict pyroxene phenocrysts (Fig. 3e) are most consistent with metaluminous suites. Phenocrysts typical of peraluminous rocks have not been observed. Alkaline affinity of the Pheno Mountain complex is supported by a high Nb/Y ratio that is typical of alkaline to peralkaline rhyolites (Fig. 6b) and by the presence of blue amphibole (Fig. 4d) and normative acmite in one trachytic dike.

U-Pb dating of zircon separated from a subvolcanic Pheno Mountain complex quartz feldspar porphyry yielded a crystallization age of 7.78 ± 0.01 Ma. This age is significantly older than the ~85 to 9 Ka Hoodoo Mountain complex (³⁹Ar/⁴⁰Ar whole rock ages: Edwards et al., 2002) precluding the tentative correlation of Mihalynuk et al. (2012). The NCVP mainly comprises alkaline mafic rocks; evolved volcanic rocks are rare (see Edwards and Russell, 2000 and references therein). However, rhyolite has been documented at Level Mountain (Hamilton, 1981) and Mount Edziza (Souther, 1992). Both of these complexes erupted felsic volcanic rocks in the Late Miocene, following construction of coalesced basaltic

Table 2. Whole Rock geochemistry of the Pheno Mountain complex.

Sample ¹	Rhyolite								Quartz feldspar porphyry				Mafic	Trachyte		
	15-1A	15-1C	606A	606B	608	610A	610B	633 ⁵	551	554	556A	636A	556B	11-6B ⁶	561	586 ⁶
N ²	56.899	56.899	56.893	56.893	56.892	56.877	56.877	56.956	56.924	56.919	56.917	56.933	56.917	56.932	56.915	56.906
W ²	131.421	131.421	131.388	131.388	131.392	131.420	131.420	131.457	131.385	131.384	131.386	131.431	131.386	131.355	131.411	131.367
SiO ₂	78.39	76.15	72.28	74.70	75.55	75.53	79.15	79.96	74.32	74.31	77.73	73.29	39.35	59.80	61.40	61.82
Al ₂ O ₃	7.82	8.94	11.33	10.44	10.80	10.85	9.89	7.32	12.11	11.25	11.59	9.67	17.18	15.44	14.29	14.30
Fe ₂ O ₃	7.38	6.72	6.79	6.09	4.75	4.27	2.87	4.21	3.51	5.14	1.54	7.44	13.45	9.03	8.14	8.84
MgO	0.01	0.02	0.06	0.09	0.02	0.02	BD	0.01	0.09	0.16	0.07	0.07	3.15	0.28	0.08	0.36
CaO	0.04	0.02	0.08	0.09	0.12	0.16	0.06	0.06	0.14	0.09	0.11	0.89	11.80	0.60	2.28	2.13
Na ₂ O	0.14	0.14	0.15	0.17	0.28	1.46	4.03	1.78	3.70	0.13	2.64	2.38	2.40	4.77	2.96	5.10
K ₂ O	4.32	5.55	7.54	6.73	5.86	6.16	2.24	3.08	5.11	5.52	5.47	3.99	0.77	5.74	6.87	5.58
TiO ₂	0.26	0.30	0.39	0.36	0.25	0.25	0.20	0.21	0.27	0.30	0.08	0.32	2.50	1.05	0.62	0.71
P ₂ O ₅	0.01	0.02	0.04	0.03	BD ⁴	0.01	BD	0.02	0.03	0.02	BD	0.02	0.47	0.32	0.11	0.14
MnO	0.12	0.13	0.13	0.12	0.06	0.08	BD	0.06	0.06	0.06	0.03	0.13	0.20	0.22	0.23	0.24
LOI	1.20	1.70	1.00	1.00	1.90	0.90	1.30	2.50	0.50	2.50	0.70	1.20	8.40	2.50	2.80	0.60
Sum	99.70	99.64	99.79	99.83	99.58	99.72	99.80	99.16	99.85	99.45	99.93	99.45	99.69	99.71	99.83	99.86
Ba (ppm)	16	11	52	55	13	28	38	18	205	1468	39	66	458	1350	614	335
Cs	0.50	0.90	0.50	0.70	2.80	1.20	0.70	1.00	0.90	1.60	1.40	1.10	2.30	2.20	5.50	0.60
Ga	36.8	43.5	47.0	41.7	42.1	35.0	38.2	22.3	34.1	36.8	23.2	50.6	21.6	30.4	28.9	32.6
Hf	37.3	43.2	30.1	22.7	45.2	31.5	28.0	83.4	15.2	42.3	8.1	50.0	3.6	12.1	8.4	9.6
Nb	162	221	132	143	200	140	121	302	57	171	77	205	21	55	46	49
Pb	45.0	35.8	14.7	6.8	36.4	32.5	18.1	77.8	5.2	26.1	11.3	20.4	2.1	7.8	10.9	7.4
Rb	148	213	232	243	220	256	98	120	116	186	206	189	13	103	98	64
Sr	4.8	3.7	8.5	7.8	5.4	8.8	7.9	5.7	18.7	365	29.2	44.9	816	142.4	36.1	37.4
Ta	11.5	13.4	8.5	7.4	12.9	9.2	8.3	21.1	3.7	11.2	6.4	12.6	1.5	3.4	2.5	3.4
Th	25.5	28.1	18.2	13.8	27.1	26.8	25.7	56.6	11.2	28.2	30.5	37.4	1.7	8.2	5.9	5.8
U	6.1	11.7	6.2	3.3	10.9	8.8	10.0	22.1	4.8	11.6	13.6	13.4	0.5	3.2	1.3	2.2
Zr	1442	1872	1081	949	1893	1211	1096	3110	576	1627	148	2016	162	471	359	368
Y	144	201	108	98	199	149	110	453	71	166	71	255	29	63	48	56
La	126.1	71.3	64.9	44.1	198.5	190.2	40.4	432.7	60.3	101.7	14.1	212.2	21.4	48.1	60.3	47.6
Ce	201.4	154.0	121.6	93.0	398.4	311.3	80.0	844.6	126.6	216.9	74.1	448.0	44.6	106.5	99.5	101.5
Pr	34.82	20.62	18.08	11.12	52.86	42.22	9.60	106.60	16.74	28.36	3.68	51.86	6.15	13.80	14.56	13.58
Nd	130.6	84.7	68.7	44.1	202.5	155.6	34.8	420.3	66.1	107.2	13.3	206.9	28.3	55.2	55.5	54.4
Sm	28.88	24.95	15.08	9.74	40.48	29.17	7.83	86.26	13.92	23.57	4.01	44.86	6.19	12.54	10.99	11.95
Eu	1.60	1.69	1.19	0.85	1.85	0.94	0.31	4.11	0.95	1.04	0.06	2.62	2.06	3.14	2.54	2.38
Gd	26.74	30.35	14.39	11.23	36.90	27.06	10.30	86.40	13.17	23.11	5.69	47.19	6.06	11.98	9.83	11.21
Tb	4.43	5.66	2.67	2.37	5.95	4.07	2.19	13.29	2.19	4.13	1.38	8.05	0.90	1.91	1.65	1.78
Dy	28.34	34.95	19.48	16.32	35.13	26.62	17.49	86.69	13.56	29.18	10.19	45.82	5.34	12.70	9.21	10.75
Ho	5.39	7.33	3.91	3.59	6.90	4.97	3.84	15.87	2.64	5.88	2.26	10.45	0.99	2.29	1.77	1.97
Er	14.39	21.56	12.05	11.17	19.92	14.34	11.98	45.55	7.38	18.38	7.17	27.18	2.75	6.47	4.96	5.86
Tm	2.31	3.19	1.86	1.66	2.96	2.21	1.86	6.39	1.17	2.79	1.16	4.28	0.38	0.95	0.77	0.86
Yb	15.57	20.71	12.45	10.73	19.57	14.57	12.56	41.47	7.23	18.78	8.36	25.90	2.38	6.05	5.11	5.64
Lu	2.16	3.01	1.81	1.65	2.64	2.00	1.76	5.50	1.07	2.63	1.14	3.86	0.38	0.89	0.80	0.87
Ce/Ce* ³	0.75	0.98	0.87	1.03	0.95	0.85	1.00	0.96	0.98	0.99	2.52	1.05	0.95	1.01	0.82	0.98
Eu/Eu*	0.18	0.19	0.25	0.25	0.15	0.10	0.11	0.15	0.21	0.14	0.04	0.17	1.03	0.78	0.75	0.63
Nb/Nb*	0.96	1.66	1.29	1.95	0.92	0.66	1.26	0.65	0.74	1.08	1.25	0.78	1.17	0.94	0.82	1.00

1. Sample numbers 11-6B, 15-1A, 15-1c are preceded by MMI-11; all other samples are preceded by ZE11. 2. Geographic coordinates, NAD 83, decimal degrees

3. Chondrite-normalized values (Sun and Macdonough, 1989) Ce*=(La_n*Pr_n)^{0.5}; Eu*=(Sm_n*Gd_n)^{0.5}; Nb*=(Th_n*La_n)^{0.5}. 4. BD - Below Detection; 5 - boulder; 6 - dike

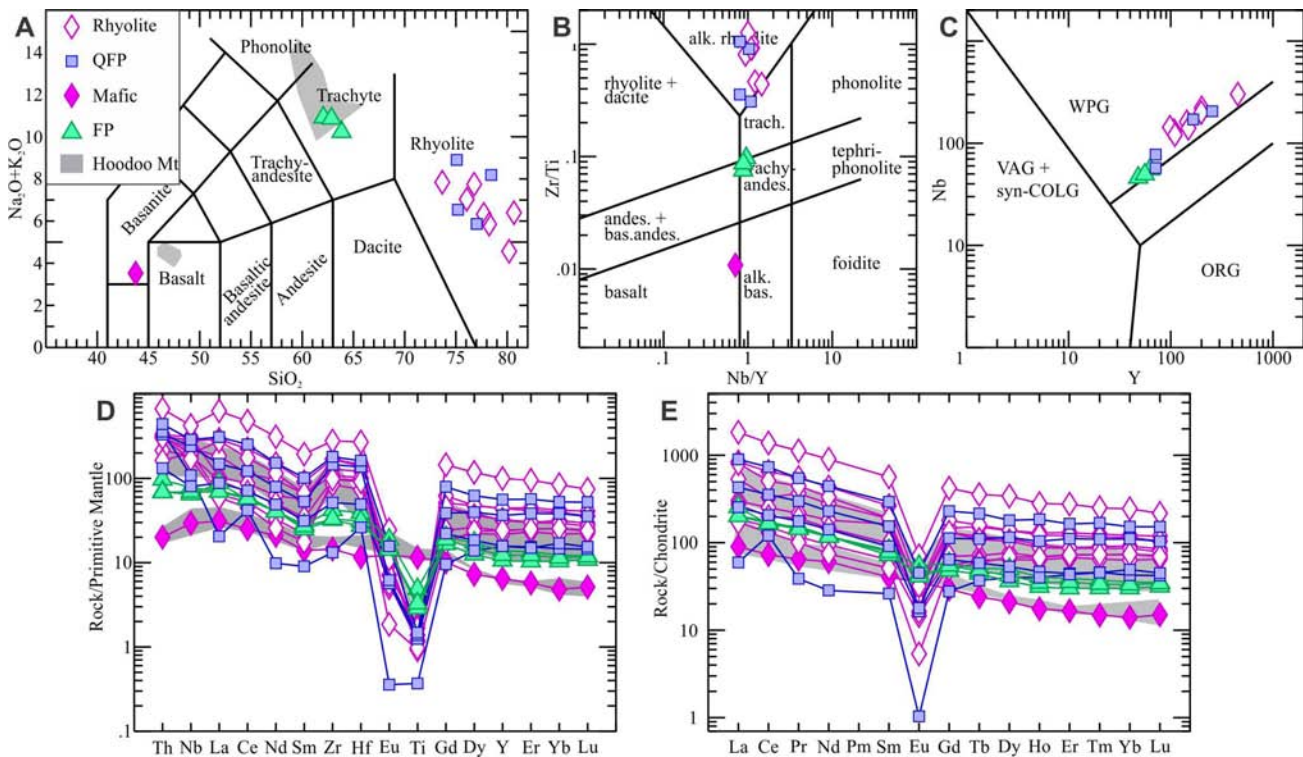


Fig. 6. Geochemical characteristics of the Pheno Mountain complex. **a)** TAS plot (Le Maitre et al., 1989); QFP – quartz feldspar porphyritic dikes, FP – feldspar porphyry. **b)** Pearce (1996) rock type plot. **c)** Felsic discrimination plot (Pearce et al., 1984). **d)** and **e)** Extended trace element plots. Normalization factors from Sun and McDonough (1989). Fields of Hoodoo Mountain complex are plotted for reference (from Edwards et al., 2002)

shields (Hamilton, 1981; Souther, 1992; Edwards and Russell, 2000). The Pheno Mountain complex is temporally equivalent to silica-saturated metaluminous to peralkaline rhyolitic rocks at Level Mountain and Mount Edziza, but apparently erupted directly onto Mesozoic basement, without construction of an extensive basaltic shield (Fig. 7). The lack of eruptive basaltic products thus presents a bit of a conundrum for the generation of these highly fractionated melts. Whereas it is possible that the Late Miocene Mount Edziza complex was much more laterally extensive than at present (Fig. 1), it is unlikely to

have been the source of the rhyolite in the Pheno Mountain complex as the present edge of the Mount Edziza complex is more than 60 km distant (Fig. 1). It is more likely that the Pheno Mountain complex was either sourced from a distinct, fractionating magma chamber or formed by low degree partial melting of the lower crust.

6. Conclusions

The Pheno Mountain complex comprises high Nb, Zr rhyolite, quartz feldspar porphyry and trachyte that unconformably overlie deformed Mesozoic to Paleozoic

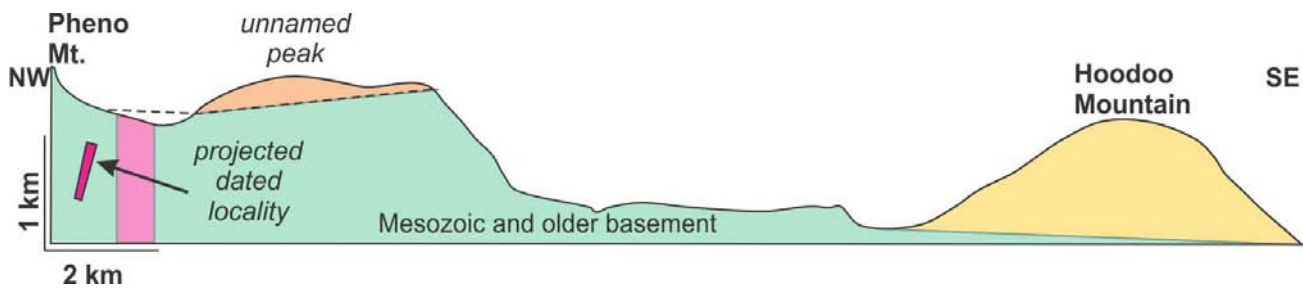


Fig. 7. Schematic NW-SE cross-section showing the relationship between Hoodoo Mountain and Pheno Mountain complexes (2x vertical exaggeration).

basement of Stikine terrane. The 7.78 Ma U-Pb zircon age confirms that the Pheno Mountain complex forms part the Neogene to Quaternary Northern Cordilleran Volcanic Province (Edwards and Russell, 2000). Because most of the NCVP was dated using K-Ar, Rb/Sr and fission track methodology (e.g., Hamilton, 1981; Souther, 1992; Evenchick and Thorkelson, 2005), which are sensitive to post-crystallization alteration and heating, the ca. 7.78 Ma age provides one of the best constraints on the NCVP felsic magmatism. Whole rock geochemistry indicates that different components of the complex are comagmatic, resolving ambiguities in field relationships. Whereas, most of NCVP is characterised by basaltic magmatism with minor felsic volcanic rocks, the Pheno Mountain complex appears unique in that it is not intimately linked to a major basaltic shield-building event.

Acknowledgments

This is a contribution to the Geological Survey of Canada Geomapping for Energy and Minerals Program (Multiple Metals Northwest Cordillera project; Geological Survey of Canada contribution #20120328). C. Evenchick, T. Hamilton, and L. Aspler are gratefully acknowledged for careful reviews that improved this paper.

References cited

- Edwards, B.R., and Russell, J.K. 2000. Distribution, nature, and origin of Neogene-Quaternary magmatism in the northern Cordilleran volcanic province, Canada. *Geological Society of America Bulletin*, 112, 1280-1295.
- Edwards, B.R., Russell, J.K., and Anderson, R.G. 2002. Subglacial, phonolitic volcanism at Hoodoo Mountain Volcano, northern Canadian Cordillera. *Bulletin of Volcanology*, 64, 254-272.
- Evenchick, C.A., and Thorkelson, D.J. 2005. Geology of the Spatsizi River map area, north-central British Columbia. *Geological Survey of Canada Bulletin* 577, 277 p.
- Gerstenberger, H., and Haase, G. 1997. A highly effective emitter substance for mass spectrometric Pb isotope ratio determinations. *Chemical Geology*, 136, 309-312.
- Gradstein, F.M., Ogg, J.G., Schmitz, M., Ogg, G., 2012, *The Geologic time scale*, Elsevier.
- Hamilton, T.S. 1981. Late Cenozoic alkaline volcanics of the Level Mountain Range, northwestern British Columbia: Geology, petrology, and paleomagnetism. University of Alberta, Edmonton, 490 p.
- Jaffey, A.H., Flynn, K.F., Glendenin, L.E., Bentley, W.C., and Essling, A.M. 1971. Precision Measurement of Half-Lives and Specific Activities of ^{235}U and ^{238}U . *Physical Review C* 4, 1889-1906.
- Kerr, F.A. 1948. Lower Stikine and western Iskut River areas, British Columbia. *Geological Survey of Canada Memoir* 246, 94 p.
- Le Maitre, R., Bateman, P., Dudek, A., Keller, J., Lameyre, J., Le Bas, M., Sabine, P., Schmid, R., Sorensen, H., Streckeisen, A., Woolley, A., and Zanettin, B. 1989. A classification of igneous rocks and glossary of terms: Recommendations of the International Union of Geological Sciences Subcommittee on the Systematics of igneous rocks Blackwell, Oxford, 193 p.
- Logan, J.M., and Koyanagi, V.M. 1994. Geology and mineral deposits of the Galore Creek area (104G/3, 4). Ministry of Energy, Mines and Petroleum Resources, British Columbia Geological Survey Bulletin 92, 95 p.
- Ludwig, K.R., 2003, *Isoplot 3.09 - A geochronological toolkit for Microsoft Excel*: Berkeley Geochronology Center, Special Publication No. 4.
- Macdonald, R. 2012. Evolution of peralkaline silicic complexes: Lessons from the extrusive rocks. *Lithos*, 152, 11-22.
- Mattinson, J.M. 2005. Zircon U-Pb chemical abrasion (CA-TIMS) method; combined annealing and multi-step partial dissolution analysis for improved precision and accuracy of zircon ages. *Chemical Geology*, 220, 47-66.
- Mihalyuk, M., Zagorevski, A., and Cordey, F. 2012. Geology of the Hoodoo Mountain area (NTS 104B/14). *Geological Fieldwork 2011*, British Columbia Ministry of Energy and Mines, British Columbia Geological Survey Paper 2012-1, 45-67.
- Mihalyuk, M., Logan, J., Zagorevski, A., and Joyce, N. 2011. Geology and mineralization in the Hoodoo Mountain area (NTS 104B/14E). *Geological Fieldwork 2010*, British Columbia Ministry of Energy and Mines, British Columbia Geological Survey Paper 2011-1, 37-63.
- Mundil, R., Ludwig, K.R., Metcalfe, I., and Renne, P.R. 2004. Age and timing of the Permian Mass Extinctions: U/Pb Dating of Closed-System Zircons. *Science*, 305, 1760-1763.
- Noble, D.C. 1970. Loss of sodium from crystallized comendite welded tuffs of the Miocene Grouse Canyon Member of the Belted Range Tuff, Nevada. *Geological Society of America Bulletin*, 81, 2677-2688.
- Pearce, J.A. 1996. A user's guide to basalt discrimination diagrams. In: *Trace element geochemistry of volcanic rocks: Applications for massive sulphide exploration*. D. A. Wyman (Ed.), Geological Association of Canada, Short Course 12, 79-113.
- Pearce, J.A., Harris, N.B.W., and Tindle, A.G. 1984. Trace element discrimination diagrams for the tectonic interpretation of granitic rocks. *Journal of Petrology* 25, 956-983.
- Schmitz, M.D., and Schoene, B. 2007. Derivation of isotope ratios, errors, and error correlations for U-Pb geochronology using ^{205}Pb - ^{235}U - ^{233}U -spiked isotope dilution thermal ionization mass spectrometric data. *Geochemistry, Geophysics, Geosystems*, 8, Q08006, 20 p.
- Scoates, J.S., and Friedman, R.M. 2008. Precise age of the platiniferous Merensky Reef, Bushveld Complex, South Africa, by the U-Pb ID-TIMS chemical abrasion ID-TIMS technique. *Economic Geology*, 103, 465-471.
- Souther, J.G. 1992. The late Cenozoic Mount Edziza volcanic complex, British Columbia. *Geological Survey of Canada, Memoir* 420, 319 p.
- Sun, S.S., and McDonough, W.F. 1989. Chemical and isotopic systematics of oceanic basalts; implications for mantle composition and processes. *Geological Society Special Publication* 42, 313-345.
- Thirlwall, M.F. 2000. Inter-laboratory and other errors in Pb isotope analyses investigated using a ^{207}Pb - ^{204}Pb double spike. *Chemical Geology*, 163, 299-322.

